Conference on Modelling Fluid Flow (CMFF'15)
The 16th International Conference on Fluid Flow Technologies
Budapest, Hungary, September 1-4, 2015

HYDRODYNAMIC MODEL OF NANOSECOND LASER ABLATION OF TUNGSTEN AND BORON

Tomasz MOSCICKI[1], Justyna CHRZANOWSKA[2]

[1] Corresponding Author. Institute of Fundamental Technological Research, Pawinskiego 5B, 02-106 Warsaw, Poland
E-mail: tmosc@ippt.gov.pl
[2] Institute of Fundamental Technological Research. E-mail: jichrzanowska@gmail.com

ABSTRACT

In this paper the interaction of Nd-YAG nanosecond laser pulse with tungsten or boron target and plasma induced during ablation are studied theoretically. Tungsten and boron were chosen because of the significant differences in their chemical and physical properties. Both materials are of a great practical importance. The model consists of equations of conservation of mass, momentum and energy and is solved with the use of commercially available program Ansys-Fluent. The calculations show the fundamental differences in ablation of both species. In case of tungsten the material evaporation is controlled by the plasma formation and consequently the absorption coefficient. The dense plasma plume can block laser radiation and limit energy transfer from the laser beam to the material. In case of boron the explosive ablation is observed. The calculations also show the sharp increase of the plume pressure after plasma formation and resulting significant increase of the velocity of plasma plume. The plume velocity obtained from the model is close to that observed in the experiment carried out in similar conditions. Moreover, the effect of laser wavelength on the quality of the deposited boron and tungsten films has been discussed on the base of ablation model.

Keywords : ablation mechanism, boron, critical temperature, plasma velocity, pulsed laser deposition, tungsten

NOMENCLATURE

a	$[m^2/s]$	thermal diffusivity
α	$[1/m]$	target absorption coefficient
C	[-]	numerical factor results from normalization
c_p	$[J\ kg^{-1}K^{-1}]$	heat capacity
F	$[J/m^2]$	laser fluence
I_L	$[W/m^2]$	laser intensity
I_0	$[W/m^2]$	peak intensity
k	$[W/m\ K]$	thermal conductivity
κ	$[1/m]$	plasma absorption coefficient
L_v	$[J/kg]$	latent heat of vaporization
λ	$[m]$	laser wavelength
$\vec{n}$	[-]	unit vector perpendicular to the surface
p	$[Pa]$	pressure
R	[-]	reflectivity
r	$[m]$	radial coordinate
ρ	$[kg/m^3]$	mass density
$s1$	$[m]$	gauss parameter (0.098×10^{-3})
$s2$	$[s]$	gauss parameter (6.0056×10^{-9})
T	$[K]$	temperature
t	[s]	time
t_0	$[s]$	time offset of the beam maximum
τ	$[s]$	laser pulse duration
$\vec{u}$	$[m/s]$	recession velocity
v	$[m/s]$	velocity
z	$[m]$	axial coordinate

Subscripts and Superscripts

c	critical
L	laser
v	vapour
s	surface
T	target

1. INTRODUCTION

In recent years growing interest in ultra-incompressible, super-hard materials (SHM) was observed. Tungsten triboride WB_3 is one of the most promising inexpensive candidate for the ultra-incompressible, super-hard materials [1-2]. Even in the form of thin films it has super-hard properties [3] and in the future may be an alternative to other hard coatings for example diamond-like DLC or cubic boron nitride (c-BN). One of the most promising methods of obtaining WB_3 films is pulsed laser deposition (PLD) because it suits very well deposition of hardly meltable metals as tungsten [4]. Pulsed laser deposition is a technique where a pulsed laser beam is focused inside a

vacuum chamber to strike a target of the material that is to be deposited. This material is ablated from the target, forms a plasma plume and subsequently deposits as a thin film on a substrate. Deposited films may have a thickness from several nanometres to several micrometres. The deposition of high quality films requires knowledge of the first step of the PLD process, which is laser ablation. The way of target ablation affect plasma plume composition, e.g. vapour to nano- and micro- particles ratio.

Besides the deposition of functional films containing boron [3,5] or tungsten [4], the laser ablation phenomenon is also used in applications such as micromachining [6], cleaning [7], and also in fabrication of micro/nanostructures [8]. Tungsten is one of very few possible materials for in-vessel components in forward looking thermonuclear reactors. Therefore, any investigation of its properties and behaviour is very important, and in particular the characterisation of its evaporation processes from the inner wall of a tokamak chamber is needed [9]. Despite of numerous applications the physics of laser ablation process is not yet thoroughly understood. It depends not only on the properties of the material, but also laser parameters such as pulse duration, frequency [6], fluence [10] and wavelength [11].

The simple mechanism of ablation consists of three stages. During the interaction of the laser beam with a material, the target is heated to a temperature exceeding its boiling temperature and sometimes, also its critical temperature. In the second stage, material evaporated from the target forms a thin layer of very dense plume, consisting of electrons, ions and neutrals. This plasma plume absorbs energy from the laser beam (by means of photoionization and inverse Bremsstrahlung) and its temperature and pressure grow. The resulting pressure gradient accelerates the plume to high velocity perpendicular to the target. At the next time steps, the laser pulse terminates and plasma plume expands adiabatically [12, 13]. This ablation pattern can be used up to some limit of fluence in which there is no phase explosion yet [10, 13]. It is assumed that the explosive boiling begins when the temperature exceeds 0.9 of the critical temperature [13]. This type of ablation results in the appearance of nano and micro particles in the plasma plume.

Therefore, detailed knowledge on laser-induced flow dynamics of plasma and understanding of the mechanisms of ablation is necessary for optimizing technological processes and promoting powerful lasers with nanosecond pulse durations for cost-effective use in industries.

In this paper the theoretical modelling of the target heating and plasma formation during interaction with nanosecond laser pulse is presented. The set of equations consists of equation of mass, momentum and energy conservation are solved with the use of Ansys Fluent software package. The main goal of the present study is a comparative analysis of the phase transition in the surface layer of a boron and tungsten target induced by nanosecond laser radiation at the wavelengths of 1064 *nm* and 355 *nm* with an intensity of 10^9 *W/cm*^{2} in vacuum. The comparison of the properties of tungsten plasmas for both laser wavelengths is presented. The simple experimental validation of theoretical model is shown.

2. THEORETICAL MODEL

The theoretical model that describes the target heating, formation of the plasma and its expansion, was previously presented in [14, 15]. The main goal of the present research is a comparative analysis of ablation mechanism of boron and tungsten target and the impact of this phenomenon on the properties of the plasma for different laser wavelengths. Calculations were made for two wavelengths of an Nd:YAG laser – 355 *nm* and 1064 *nm*. The laser beam with a Gaussian profile (10 ns FWHM) was focused to a spot size of 0,055 *mm*^{2} with a fluence of 10 *J/cm*^{2}. It was assumed that the boron or tungsten plume expands to ambient air at a pressure of 10^{-3} *Pa*. In the case of a nanosecond laser, the ablation is thermal; hence, the initial conditions for plume expansion were taken from the theory of the rapid surface vaporization [16]. Therefore, it was assumed that the vapour velocity at the end of the Knudsen layer is sonic and the other parameters are $T_v \sim 0.67\ T_s$, $p_v \sim 0.21\ p_s$, $\rho_v \sim 0.31\rho_s$ [16].

The intensity of laser beam reaching the target surface I_L was used in the form which fits the shape of the laser pulse used in our experiments

$$I_L(t,r) = \frac{CF}{\tau}\exp\left(-\left(\frac{t-t_0}{s_2}\right)^2\right)\exp\left(-\left(\frac{r}{s_1}\right)^2\right)\times\left(\exp\left(-\int \kappa dz\right)\right) \quad (1)$$

The first part of the equation (1) describes temporal evolution of the laser intensity, the second energy distribution in the laser beam and the last exponential component takes into account the attenuation of the laser beam on its way to the point (r, z) in plasma.

The laser radiation reflected from the surface of target R was included. Due to reflectance the source component in energy equation is $\kappa I_L(1+R)$ in the case of plasma, and $\alpha I_L(1-R)\exp\left(-\int \alpha dz_T\right)$ for the target. The exponential component takes into account the attenuation of the laser beam on its way to the point (r, z_T) of target.

The presented ablation model consists of two parts. The first part, which is settled with conduction equation [14, 17], was responsible for the determination of the temperature distribution and mass removal in the target. In the second part the eulerian system of equations of continuity and

the diffusion equation [14, 17] was solved for plasma.

The system of equations was solved iteratively. The target temperature was calculated and then the stream of ablated particles was determined at the end of the Knudsen layer. These conditions were taken as inlet conditions for plume expansion. Then the absorption of the laser radiation in developing plasma plume was determined and the target temperature was recalculated according to actual laser intensity at the target surface. The new target temperature was used to determine the conditions at the end of the Knudsen layer, which were subsequently used as inlet conditions for plume expansion. The other boundary conditions for plasma system of equations were as follows. The stream of boron or tungsten vapour was directed perpendicularly to the target surface. At the wall the no-slip boundary and a fixed temperature condition were applied. At the outflow boundary the pressure outlet boundary conditions [17] were used, which required the specification of a static pressure at the outlet boundary. This static pressure value is relative to the operating pressure. The axis boundary conditions were used at the centerline of the axis-symmetric geometry [17].

The boundary condition at the place where the laser beam strikes the surface of target is

$$-k\frac{\partial T_s}{\partial \vec{n}} = -\rho \vec{u}(t) L_v \qquad (2)$$

where $\vec{u}$ is the recession velocity given by the Hertz-Knudsen equation [10, 14]. Energy losses due to thermal radiation from the surface are small compared to other terms and were neglected. At other boundaries $T = 300\ K$ was assumed.

All the material functions were described in [15] and depend on the temperature in target and also on pressure and mass fraction in plasma.

For the plasma, the calculation domain was $r = 0.01\ m$ and $z = 0.025\ m$ with nonuniform grid with 60×200 nodes. The smallest computational cells had dimension of $50 \times 0.1\ \mu m$ at the vapour inlet. In the case of target the calculation domain was $r = 0.005\ m$ and $z = 2\times10^{-6}\ m$ with 130×500 nodes respectively. While the smallest computational cells had dimension of $12 \times 0.004\ \mu m$ at the target surface. The cell dimensions were fit to appearing gradients after preliminary calculations. Then it was checked that further decreasing of cell dimensions did not change the results. The time step was adjusted to the smallest cells. Both cases were time-dependent and were solved in axisymmetric geometry. In the case of the plasma, the system of equations was solved by pressure based (coupled) solver [17] with second order spatial discretization for flow. The defaults settings [17] were applied for target.

3. EXPERIMENTAL SETUP

Irradiation of a tungsten and boron targets was performed using a Nd:YAG laser (Quantel, 981 E) in a chamber evacuated to a residual pressure of $1\times10^{-5}\ Pa$. All ablation parameters were the same like in theoretical model. Both harmonics were polarized horizontally. The spatial and time profiles of the laser beam were Gaussian. The laser spot diameter defined by I_0/e^2 was determined by registration of the spot size by ICCD camera after attenuation of the laser beam and was 310 μm in the case of 1064 *nm* and 260 μm in the case of 355 *nm* wavelength. The incident angle of the laser beam was close to the surface normal. The high quality targets - boron from Kurt J. Lesker (2.35 g/cm^3 mass density, 99.5% purity) and tungsten from Kurt J. Lesker (19.35 g/cm^3, 99.95% purity) were used. Boron and tungsten thin films were deposited on a silicon (100) polished substrates (Spi Supplies) with ambient temperature. During deposition the target was rotated to avoid crater formation. The deposition time was 30 minutes (18000 pulses) for each experiment. The laser deposited films surface was subject to inspection under a Scanning Electron Microscope: JEOL, JSM-6010PLUS/LV InTouchScope™. The images of the plasma plume were registered with the use of an ICCD camera. The plasma was imaged on the camera using a 180 *cm* focal length camera lens. The image intensifier was gated for an exposure time of 5 *ns* while the delay time between the laser pulse and the pulse triggering the image intensifier was changed gradually.

4. RESULTS AND DISCUSSION

4.1. Mechanisms of Ablation

During the interaction of the laser beam with a material, the target is heated to a temperature exceeding its boiling temperature and sometimes, also its critical temperature [10,13]. Assuming a constant fluence, the different mechanisms of ablation can occur depending on the critical temperature. In the case where the target temperature is lower than $0.9\ T_c$ mainly the evaporation occurs. Above this limit the explosive boiling begins. This phenomenon causes that except electrons, ions and neutrals in the plasma plume are nano and mikro particles of the target material. Both models can be observed during the ablation of tungsten and boron, depending on the laser fluence. Due to the high critical temperature (14778 *K* [18]), and high absorption coefficients 4.4×10^7 and 8.9×10^7 *1/m* [19] respectively, for 1064 *nm* and 355 *nm* laser wavelength, tungsten is a material for which the evaporation takes place primarily for the laser intensity below $6\times10^{10}\ W/cm^2$ [20]. Figure 1 shows evolution of surface temperature at beam centre $r = 0$ for the laser

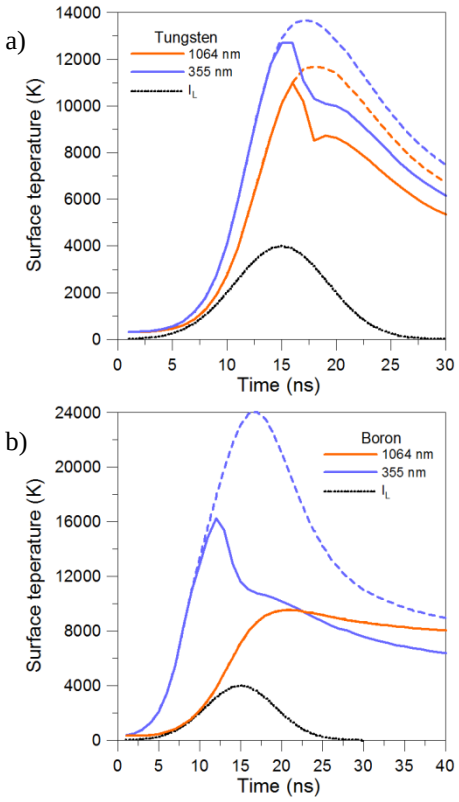

Figure 1. Target surface temperature T_s and laser intensity I_s during first 40 nanoseconds (r = 0). a) tungsten target, b) boron target. Broken line denotes case without plasma absorption.

wavelength 1064 *nm* and 355 *nm* for tungsten and boron at the laser fluence 10 J/cm^2 (10^9 W/cm^2). In the case of tungsten for the first harmonic of Nd-YAG laser the maximum surface temperature is 11700 *K* and for the third 13700 *K* (Fig. 1a).

In both cases, the maximum surface temperature is reached in 16 *ns*. At the next time steps the temperature suddenly decrease due to absorbing of the laser beam in the plasma.

The laser ablation mechanism is different in the case of boron. For both laser harmonic the maximum temperatures exceed the critical temperature (Fig. 2b), which is about 10000 *K* [18]. In this case, the explosive boiling occurs, which resulting in a film on which there are different sizes irregular shapes contaminants (Fig. 3c, d). The number and size of debris depends mainly on the optical properties of boron. In the case of λ = 1064 *nm* the absorption coefficient is 1.3×10^6 m^{-1} [21] and is a 23 times lower than for 355 *nm*. The low absorption coefficient causes that much thicker layer of material is heated, and the critical temperature is exceeded much deeper (Fig. 2). The result is an increase in the amount of larger fragments of the target in the deposited film. The maximum temperature for 1064 *nm* is obtained only in 22 *ns*. Due to the small amount of vaporized material there is practically no plasma absorption. The high maximum temperature ~19000 K is the result of failure of the model neglecting phenomenon of explosive boiling.

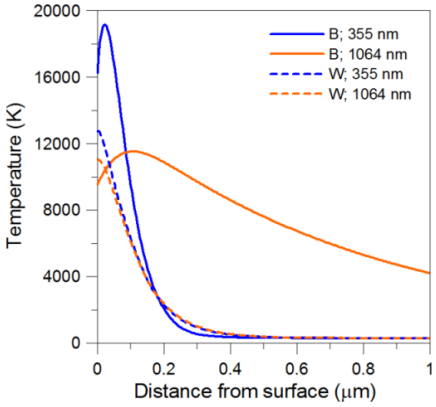

Figure 2. Target temperature T and laser intensity Is along target axis at the time moments when the surface temperature reaches its maximum value.

The rate of temperature equalization with increasing of distance over time is controlled by the coefficient of thermal diffusivity $a = k/(\rho c_p)$. Above the melting point, where it is assumed that the thermal properties and the density does not change, the value of diffusion coefficient is 2.58×10^{-5} and 1.48×10^{-6} m^2/s [15] for tungsten and boron respectively. The magnitude of this parameter indicate, that subsurface overheating of boron target is equalized much more slowly than in the case of tungsten. Moreover in the case of tungsten, in connection with larger absorption coefficients, the laser beam penetrates the target to lower depth.

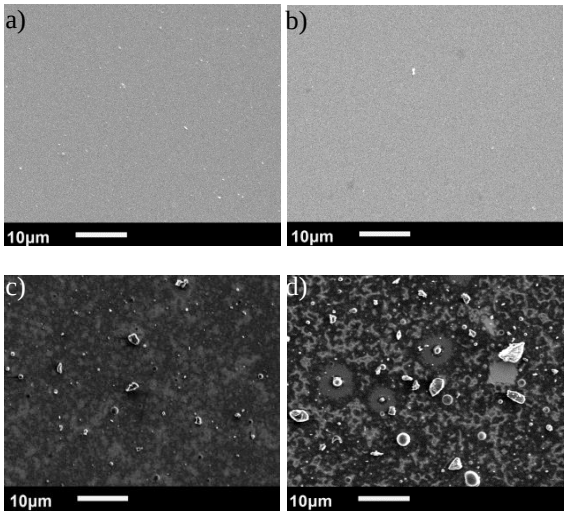

Figure 3. SEM micrograph (×1000) of deposited films: a) tungsten 1064 nm, b) tungsten 355 *nm*, c) boron 355 *nm*, d) boron 1064 *nm*. *F* = 10 *J/cm2*.

Both of these phenomena result in the maximum temperature located at the surface and the ablation process mainly by the evaporation of the

surface. As a result, the surface of deposited tungsten films is smooth (Fig. 3a, 3b).

This phenomenon is quite different in the case of boron when evaporation from the surface results in maximum of temperature placed at a certain depth. The critical temperature is achieved earlier below surface. The target surface erupts as a result of high stress. In the case of 1064 *nm* a big amount of energy is accumulated at a depth about 1 μm. Lower thermal diffusivity of boron causes the increase of target cooling time (Fig. 1b). The studies of ablation of non-metallic materials showed that the process should be carried out with a sufficiently low fluence in order to avoid the phase explosion [10, 11]. However, in the case of boron ablation with the first harmonic, such a procedure could result in temperature decrease below the critical but simultaneously could cause the lack of ablation.

4.2. Plasma Properties

The first attempt in modelling the expansion of boron and tungsten plasma plume was taken in [15]. The calculated distributions of plasmas parameters in the early phase of expansion show that plasma temperatures are higher in the case of tungsten but the velocities are higher in the case boron [15]. Differences in the distribution of velocity are logical and based on the weight difference of the two elements. In the case of the temperature distribution it was necessary to analyse absorption of laser radiation by the plasma of both elements [15]. It was assumed that the ablation process occurs only as a result of evaporation. As shown in the previous section in modelling of boron the significant approximation was used. Therefore, the effect of the laser wavelength on the behaviour of the plasma is discussed only for tungsten ablation.

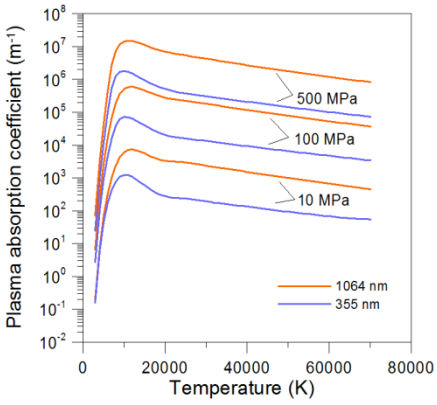

Figure 4. Absorption of 1064 *nm* and 355 *nm* laser radiation in tungsten vapour under pressure 10, 100 and 500 *MPa*.

The figure 4 shows the distribution of the absorption coefficient of tungsten for different temperatures, pressures, and laser wavelength. For

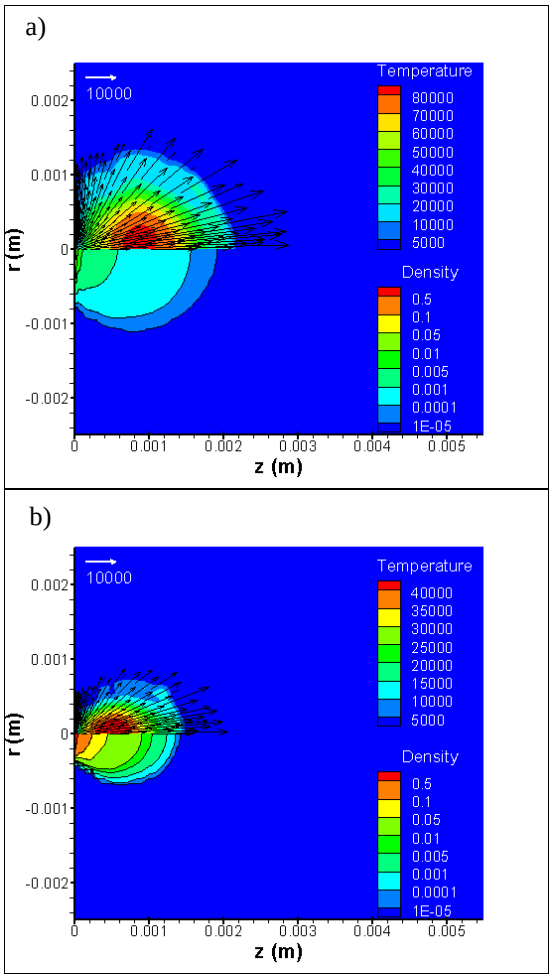

Figure 5. Distribution of density, temperature and velocity in plasma induced during laser ablation of tungsten 100 *ns* after the beginning of the laser pulse for a)1064 *nm* and b) 355 *nm* laser wavelength.

the pressure 10^8 *Pa* the absorption coefficient of 355 *nm* laser radiation is 8.4 times lower than that of 1064 *nm*. This affects the plasma ignition timing and its properties. The calculated distributions of plasma temperature and pressure after 100 *ns* of expansion (Fig. 5) show that plasma temperatures are higher in the case of 1064 *nm* but the pressures and densities are higher in the case of 355 *nm*, which is in agreement with experimental findings [11, 22]. Smaller penetration depth and reflection coefficient *R* in the case of 355 *nm* causes a higher surface temperature of the target, and thus the greater the rate of ablation. The greater ablation rate results in larger mass density of the ablated plume and hence, in higher pressures. An additional consequence of a higher ablation rate is slower expansion and smaller dimensions of the plasma plume. Higher plasma temperature in the case of 1064 *nm* is the result of lower density and stronger plasma absorption. At 100 *ns* after the beginning of the laser pulse the maximum temperature for the third harmonic is 2 times lower

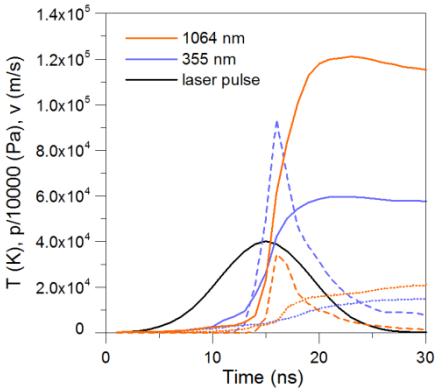

Figure 6. Tungsten plasma parameters during 30 *ns* after the beginning of laser pulse (at *r* = 0) for 1064 *nm* and 355 *nm* wavelenght. Dotted line- velocity, broken - pressure and solid – temperature.

than in the case of the first harmonic of laser irradiation and is about 45000 *K*.

The distribution of tungsten plasma parameters during 30th *ns* after the beginning of laser pulse at *r* = 0 is shown in Figure 6. As it was discussed in previous works, the acceleration of the plasma is caused by the hydrodynamic effects [23]. The same is in the case of tungsten. To about 15th *ns* pressure increases and there is the plasma ignition.

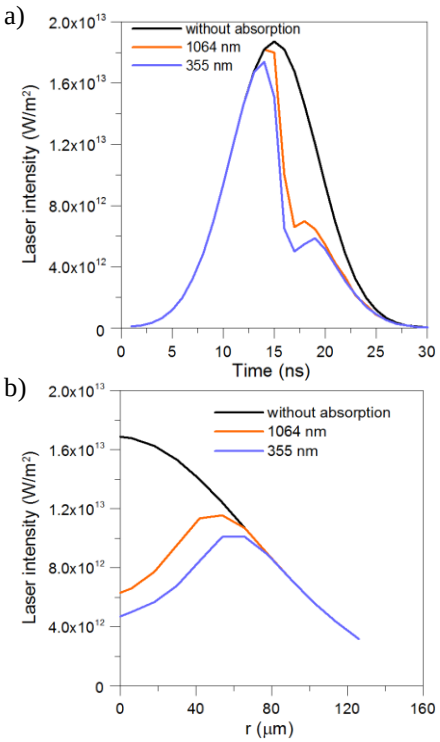

Figure 7. Distribution of laser intensity for 1064 *nm* and 355 *nm* laser wavelength: a) on the axis during laser pulse and b) radial distribution at *t* = 17 *ns*.

Due to the large difference in absorption coefficients depending on the wavelength of the laser, the ignition in the case of 1064 *nm* occurs at a pressure of about 3×10^8 *Pa* which is three times lower than that for 355 *nm*. In the next time steps, the pressure decreases rapidly causing the acceleration of plasma plume. The decrease in density due to the expansion and intensive absorption of energy from the laser beam causes a rapid increase of temperature and velocity. After 30 *ns*, the velocity of the plume ablated by 355 *nm* is 14850 *m/s* while the velocity of the plume ablated by 1064 *nm* reaches 20750 *m/s* (Fig. 6).

For 10 J/cm^2 the total absorption of laser beam is at the level of 6% in the case of 355 *nm* radiation and about 3.5% in the case of 1064 *nm*. As shown in Fig. 7a the decrease in intensity of laser radiation due to laser absorption occurs just before the pulse maximum, e.g.. in 13th *ns* in the case of 355 *nm* and 14th *ns* respectively for 1064 *nm*. In both cases, the maximum of absorption is in 17th ns, and is the biggest on the axis of the plasma (Fig. 7b). Greater value of the absorbed energy for third harmonic is due to the earlier ignition, and higher absorption coefficient which strongly grow with increase of plasma pressure (Fig. 4).

4.3. Experimental validation

The plasma plume propagation was studied by optical imaging at 80-400 *ns* time delay after the laser shot. The images of tungsten plasma at delay time 100 *ns* for 355 *nm* and 1064 *nm* are presented in the figure 8.

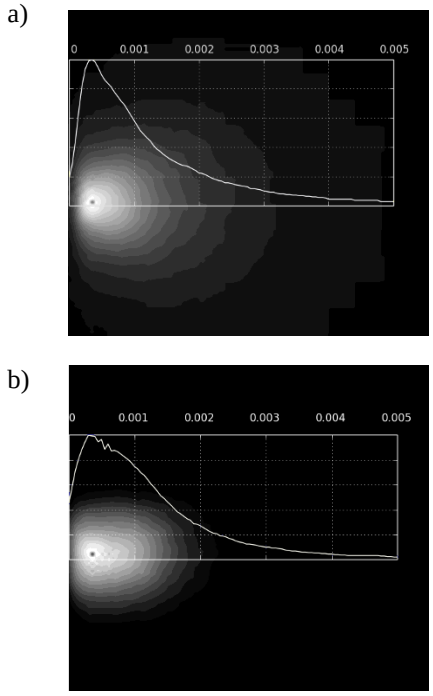

Figure 8. ICCD images of tungsten plasma at delay time 100 ns for a) 1064 *nm* and b) 355 *nm*. Solid line denotes the intensity distribution of plasma radiation on the axis of plasma *r* = 0.

For every single image of plasma plume the half-Lorentzian plot was fitted to on axis intensity. The Lorentzian plot position is taken as a maximum intensity of plasma plume and FWHM is a level of plasma expansion. Figure 9 presents Tungsten plasma position and FWHM of Lorentzian plot fitted to plasma intensity distribution.

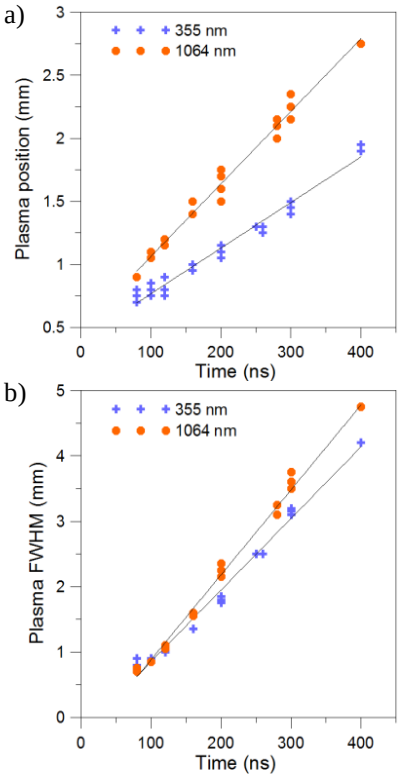

Figure 9. Experimental tungsten plasma plume parameters for 1064 and 355 nm laser wavelengths a) velocity of plasma propagation and b) velocity of plasma expansion

On the basis of plasma propagation and expansion in time were calculated the plasma displacement and expansion velocity, respectively. Total velocity of plasma front is defined as a sum of both velocities mentioned above. Results are presented in table 1.

Table 1. Comparison of tungsten plasma velocity for different wavelength.

Velocity [*m/s*]	355 *nm*	1064 *nm*
Plasma displacement	3580	5800
Plasma expansion	10545	13000
Total	14125	18800

The quantitative comparison of the experimental plasma shape with the theoretical results is rather difficult because the images show plasma radiation which depends both on plasma density and temperature. However, plasma dimensions are similar; for example after 100 *ns* the tungsten plasma diameter is about 2 *mm*. The front velocities obtained from the experimental plasma images are only 10 % lower than the calculated in model.

5. SUMMARY

In this paper the interaction of Nd-YAG nanoseconds laser beam with tungsten or boron target and induced during ablation plasma are studied theoretically. The calculations show the fundamental differences in ablation of both species. In case of tungsten the evaporation of material is controlled by the plasma formation and consequently the absorption coefficient. The dense plasma plume can block laser radiation and limit energy transfer from the laser beam to the material. In case of boron the explosive ablation is observed. Such behaviour is affected by subsurface heating and transition to super critical state. In the case of 1064 *nm* wavelength the effect is magnified by the high penetration depth of the laser beam. Therefore, in ceramics target with a boron excess [1, 24], there may be adverse phenomena which impact on the quality of the deposited film.

The calculations show considerable increase of the velocity of plasma plume due to hydrodynamic effects. In the case of laser ablation of tungsten with the wavelength of 1064 *nm* the plasma plume has a higher energy due to the higher temperature and velocity in comparison with 355 *nm*. At the same time less material is transported in the plume. Both of these parameters are responsible for the deposition rate of the film and its adhesion. The plume velocity obtained from the model is close to that observed in the experiment carried out in similar conditions.

Finally, it should be noted that the presented model is not appriopriate for fluences causing exceed of critical temperature in the subsurface region. However, the use of partial results help to explain the phenomena occurring during nanoseconds laser ablation.

ACKNOWLEDGEMENTS

This work was supported by the National Science Centre (Poland). Research Project: UMO-2012/05/D/ST8/03052

REFERENCES

[1] Mohammadi, R., Lech, A.T., Xie, M., Weaver, B.E., Yeung, M.T., Tolbert, S.H. and Kaner, R. B., 2011, "Tungsten Tetraboride, an Inexpensive Superhard Material", *Proc Natl Acad Sci* Vol. 108 (27), pp. 10958-10962.

[2] Liang, Y., Fu, Z., Yuan, X., Wang, S., Zhong, Z., and Zhang, W., 2012, "An Unexpected Softening from WB_3 to WB_4", *Europhys Lett*, Vol. 98, pp. 66004.

[3] Rau, J.V., Latini, A., Teghil, R., De Bonis, A., Fosca, M., Caminiti, R., Rossi Albertini, V., 2011, "Superhard Tungsten Tetraboride Films Prepared by Pulsed Laser Deposition Method", *ACS Appl Mater Interfaces*, Vol. 3, pp. 3738–3743.

[4] Dellasega, D., Merlo, G., Conti, C., Bottani C. E., and Passoni, M., 2012, "Nanostructured and Amorphous-like Tungsten Films Grown by Pulsed Laser Deposition", *J Appl Phys*, Vol. 112, pp. 084328

[5] Friedmann, T. A., McCarty, K. F., Klaus, E. J., Barbour, J. C., Clift, W. M., Johnsen, H. A., Medlin, D. L., Mills, M. J., and Ottesen, D. K., 1994, "Pulsed Laser Deposition of BN onto Silicon (100) Substrates at 600˚C", *Thin Solid Films*, Vol. 237, pp. 48-56.

[6] Bulgakova, N.M., Zhukov, V.P., Collins, A.R., Rostohar, D., Derrien, T. J.-Y., and Mocek T., 2015, "How to Optimize Ultrashort Pulse Laser Interaction with Glass Surfacesin Cutting Regimes?", *Appl Surf Sci*, doi:10.1016/j.apsusc.2014.12.142

[7] Kubkowska, M., Gasior, P., Rosinski, M., Wolowski, J., Sadowski, M.J., Malinowski, K., and Skladnik-Sadowska, E. 2009, "Characterisation of Laser-Produced Tungsten Plasma Using Optical Spectroscopy Method", *Eur Phys J D*, Vol. 54, pp. 463–466.

[9] Jong-Won Yoona, and Kwang Bo Shim, 2011, "Growth of Crystalline Boron Nanowires by Pulsed Laser Ablation", *J Ceram Procces Res*, Vol. 12(2), pp. 199-201.

[8] Afif, M., Girardeau-Montaut, J.P., Tomas, C., Romand M., Charbonnier M., Prakash, N.S., Perez, A., Marest, G., and J.M. Frigerio, 1996, "In Situ Surface Cleaning of Pure and Implanted Tungsten Photocathodes by Pulsed Laser Irradiation", *Appl Surf Sci*,Vol. 96-98, pp. 469-473.

[10] Bulgakova, N.M., and Bulgakov, A.V., 2001, „Pulsed Laser Ablation of Solids: Transition from Normal Vaporization to Phase Explosion", *Appl. Phys. A*, Vol. 73(2), pp. 199-208

[11] Hoffman, J., Chrzanowska, J., Kucharski, S., Moscicki, T., Mihailescu, I.N., Ristoscu, C., and Szymański, Z., 2014, "The Effect of Laser Wavelength on the Ablation Rate of Carbon", *Appl Phys A*, Vol. 117, pp. 395-400

[12] Singh, R.K., and Narayan, J., 1990, "Pulsed-laser Evaporation Technique for Deposition of Thin Films: Physics and Theoretical Model", *Phys Rev B*, Vol. 41, pp. 8843-8859.

[13] Kelly, R., and Miotello, A., 1996, "Comments on Explosive Mechanisms of Laser Sputtering", *Appl Surf Sci*, Vol. 96-98, pp. 205-215.

[14] Moscicki, T., Hoffman, J., and Szymanski, Z., 2013, "The effect of laser wavelength on laser-induced carbon plasma", *J Appl Phys*,Vol. 114, pp. 083306.

[15] Moscicki, T., 2014, "Expansion of laser-ablated two-component plume with disparate masses", *Phys Scripta*, Vol. T161, pp. 014024.

[16] Knight, C. J., 1979 , "Theoretical Modelling of Rapid Surface Vaporization with Back Pressure", *AIAA Journal*, Vol. 17, pp.519-523.

[17] ANSYS® Academic Research, Release 15.0, Help System, Fluent Documentation, ANSYS, Inc.

[18] Blairs, S., and Abbasi M., H., 2006, "Correlation Between Surface Tension and Critical Temperatures of Liquid Metals", *J Colloid Interf Sci*, Vol. 304, pp. 549–553

[19] Rakic, A. D., Djurisic, A. B., Elazar, J. M., and Majewski, M. L., 1998, "Optical Properties of Metallic Films for Vertical-cavity Optoelectronic Devices", *Appl Opt*, Vol. 37, pp. 5271-5283

[20] Yahiaoui, K., Kerdja, T., and Malek, S., 2010, "Phase Explosion in Tungsten Target under Interaction with Nd : YAG Laser Tripled in Frequency", *Surf Interface Anal*, Vol. 42, pp. 1299–1302

[21] Morita, N., and Yamamoto, A., 1975,"Opticaland Electrical Properties of Boron", *Jpn J Appl Phys*, Vol. 14, pp. 6

[22] Hussein, A.E., Diwakar, P.K., Harilal, S.S., and Hassanein, A., 2013 ,"The Role of Laser Wavelength on Plasma Generation and Expansion of Ablation Plumes in Air", *J Appl Phys*, Vol. 113, pp. 143305

[23] Hoffman, J., Moscicki, T., and Szymanski, Z., 2012, "Acceleration and Distribution of Laser-Ablated Carbon Ions Near the Target Surface", *J Phys D Appl Phys*, Vol. 45, pp. 025201

[24] T., Moscicki, J., Hoffman, J., Radziejewska, J., Chrzanowska, N., Levintant-Zayonts, and D., Garbiec, 2014, "Formation of WB_4 Thin Films Using Nanosecond Nd-YAG Laser", Book of Abstracts, 4th National Conference on Nano- and Micromechanics, Wroclaw, Poland, pp.152-154.